View metadata, citation and similar papers at core.ac.uk

brought to you by CORE

provided by DigitalCommons@University of Nebraska

University of Nebraska - Lincoln

DigitalCommons@University of Nebraska - Lincoln

C.J.G.J. Uiterwaal Publications

Research Papers in Physics and Astronomy

9-19-2005

Creation of optical vortices in femtosecond pulses

I. G. Mariyenko
University of Nebraska - Lincoln

James Strohaber
University of Nebraska-Lincoln, jstroha1@gmail.com

Cornelis J. Uiterwaal
University of Nebraska - Lincoln, cuiterwaal2@unl.edu

Follow this and additional works at: https://digitalcommons.unl.edu/physicsuiterwaal

Part of the Physics Commons

Mariyenko, I. G.; Strohaber, James; and Uiterwaal, Cornelis J., "Creation of optical vortices in femtosecond pulses" (2005). *C.J.G.J. Uiterwaal Publications*. 13.
https://digitalcommons.unl.edu/physicsuiterwaal/13

This Article is brought to you for free and open access by the Research Papers in Physics and Astronomy at DigitalCommons@University of Nebraska - Lincoln. It has been accepted for inclusion in C.J.G.J. Uiterwaal Publications by an authorized administrator of DigitalCommons@University of Nebraska - Lincoln.

Creation of optical vortices in femtosecond pulses

I. G. Mariyenko, J. Strohaber, and C. J. G. J. Uiterwaal

Department of Physics & Astronomy, The University of Nebraska-Lincoln, Behlen Lab - City Campus, Lincoln, NE 68588-0111
imariyenko3@unl.edu , cuiterwaal2@unl.edu

Abstract: We experimentally created a femtosecond optical vortex using a pair of computer-synthesized holographic gratings arranged in a $2f$-$2f$ optical setup. We present measurements showing that the resulting donut mode is free of spatial chirp, and support this finding with an analysis of the optical wave propagation through our system based on the Kirchhoff-Fresnel diffraction integral. An interferogram confirms that our ultrashort vortex has topological charge 1, and a conservative experimental estimation of its duration is 280 fs. We used 25-fs radiation pulses (bandwidth approximately 40 nm) produced by a Ti:sapphire laser oscillator.

© 2005 Optical Society of America

OCIS codes: (090.1760) Computer holography; (050.1590) Chirping; (050.1950) Diffraction gratings; (140.3300) Laser beam shaping; (320.7090) Ultrafast lasers; (999.9999) Optical vortices.

References and Links

1. J.F. Nye and M.V. Berry, "Dislocation in wave trains," Proc. Roy. Soc. London, Ser. A, Math. Phys. Sc. **336,** 165–190 (1974).
2. A.E. Siegman, *Lasers* (University Science Books, Sausalito, CA, 1986).
3. L. Allen, M.W. Beijersbergen, R.J.C. Spreeuw, and J.P. Woerdman, "Orbital angular momentum of light and the transformation of Laguerre-Gaussian laser modes," Phys. Rev. A **45,** 8185–8189 (1992).
4. P. B. Corkum, "Plasma perspective on strong field multiphoton ionization," Phys. Rev. Lett. **71,** 1994–1997 (1993).
5. A. Scrinzi and H. G. Muller, "Attosecond pulses: generation, detection, and applications," in *Strong Field Physics*, T. Brabec and H.C. Kapteyn, eds. (Springer 2004).
6. D.N. Fittinghoff, P.R. Bolton, B. Chang, and K.C. Kulander, "Polarization dependence of tunneling ionization of helium and neon by 120-fs pulses at 614 nm," Phys. Rev. A **49,** 2174–2177 (1994).
7. K. Bezuhanov, A. Dreischuh, G.G. Paulus, M.G. Schätzel, and H. Walther, "Vortices in femtosecond laser fields," Opt. Lett. **29**, 1942–1944 (2004).
8. V.Yu. Bazhenov, M.V. Vasnetsov, and M.S. Soskin, "Laser beams with screw dislocations in their wavefronts," Pis'ma Zh. Eksp. Teor. Fiz. **52,** 1037–1039 (1990).
9. N.R. Heckenberg, R. McDuff, C.P. Smith, and A.G. White, "Generation of optical phase singularities by computer-generated holograms," Opt. Lett. **17,** 221–223 (1992).
10. C.P. Smith, R.G. McDuff, N.R. Heckenberg, M.S. Soskin, and M.V. Vasnetsov, "Experimental realisation and detection of optical vortices," in *Optical Vortices* (Vol. 228 Horizons in World Physics), M. Vasnetsov and K. Staliunas, eds. (Nova Science, Commack, NY, 1999).
11. J. Arlt, K. Dholakia, L. Allen, and M.J. Padgett, "The production of multiringed Laguerre-Gaussian modes by computer-generated holograms," J. Mod. Opt. **45,** 1231–1237 (1998).
12. see for instance E. Hecht, *Optics* (Addison Wesley Longman, Reading, MA, 1998).
13. see http://www.corning.com
14. B. J. Pearson, J. L. White, T. C. Weinacht, and P. H. Bucksbaum, "Coherent control using adaptive learning algorithms," Phys. Rev. A **63,** 063412 (2001).

1. Introduction

An optical vortex, as defined for a scalar electric field, is a singularity point where the amplitude vanishes and the phase is undetermined. The phase circulation around the

singularity point is an integer (m) multiple of 2π [1]. This integer m is called the *topological charge* of the vortex. Laguerre-Gaussian modes [2,3], characterized by their two mode indices p (radial index) and ℓ (azimuthal index) are well-known examples of radiation modes containing an optical vortex; they have topological charge $m = \ell$. They typically consist of one or more concentric rings of intensity, with the vortex core located at the center, so that the intensity must vanish there. The archetypical Laguerre-Gaussian mode is the one with $p = 0$ and $\ell = 1$. Figure 1 shows the amplitude and phase in the waist of this mode. The intensity is located on a single ring, which explains why this mode is often nicknamed "donut mode".

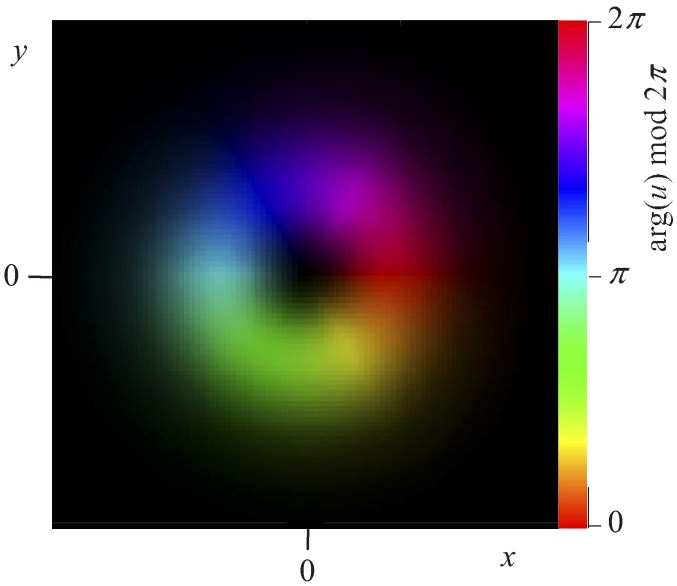

Fig. 1. Snapshot of the amplitude and phase of the scalar electric field $u = |u| \exp(i \arg(u))$ in a transversal plane through the waist of a Laguerre-Gaussian mode with radial index $p = 0$ and azimuthal index $\ell = 1$ (donut mode). The axis of propagation z is perpendicular to the plane of the drawing, and passes through the center at $(x,y) = (0,0)$. The brightness of the picture indicates the magnitude-squared amplitude $|u|^2$ of the field; the color indicates the phase angle $\arg(u) = -\ell\varphi$ according to the color strip on the right [$\varphi = \arctan(y/x)$ is the azimuthal angle in the plane of the drawing].

Our interest in this sort of mode stems from the fact that they possess optical orbital angular momentum. For instance, photons in a Laguerre-Gaussian mode carry an orbital angular momentum of $\ell\hbar$ per photon [3]. Ultimately, our goal is to have strong ultrashort radiation pulses containing an optical vortex, so that we can investigate the influence of optical orbital angular momentum on intense-field ionization processes. We are motivated by what is known about the role of the photon's spin angular momentum. This manifests itself as the polarization of radiation, which is well known to affect intense-field ionization processes. Notable in this context are electron recollision processes [4], which play a crucial role in many currently exploited or investigated techniques to generate attosecond pulses [5]: electron recollision is more likely for linear than for circular polarization [6]. What role optical orbital angular momentum plays in intense field atomic processes is to the best of our knowledge experimentally unexplored territory.

For ionization research in this area we need pulses that are both intense and ultrashort, and contain an optical vortex. The strategy we have chosen to create these is to first endow a weak

#7943 - $15.00 USD Received 1 July 2005; revised 9 September 2005; 12 September 2005
(C) 2005 OSA

but ultrashort pulse with a vortex, and then to amplify it to the required energy level (mJ/pulse). In this paper, we report on the first step: creating a vortex in weak pulses of femtosecond duration. Femtosecond pulses naturally have a large bandwidth, so that none of the techniques reported to generate vortices in monochromatic (narrowband) light is suitable. A short overview of these techniques can be found in Ref. [7]. To the best of our knowledge, Ref. [7] is also the only paper published that presents an experimental realization of vortices in femtosecond laser fields. It seems, however, that the folded 4*f* setup employed by the authors of Ref. [7] leaves a role for parasitic reflections, which they mention as a complicating factor, and that the alignment of their setup is more critical than it is for ours. As a consequence, the intensity in the center of their resulting donut mode does not fall below 20% of the intensity on the donut ring, while ideally the intensity has to vanish at the center because that is where the vortex core is located. In contrast, our present setup produces donut modes with a clean dark center (see Fig. 4(d) below) while still handling the large bandwidth of ultrashort pulses.

This paper is organized as follows. In Sec. 2 we describe our experimental setup. This is followed in Sec. 3 by wavefront propagation calculations showing that our setup produces optical vortices of ultrashort duration. After that, in Sec. 4, we present experimentally recorded images and interferograms of our produced ultrashort vortex-containing donut modes, and an experimental estimation of their duration; this is followed by conclusions.

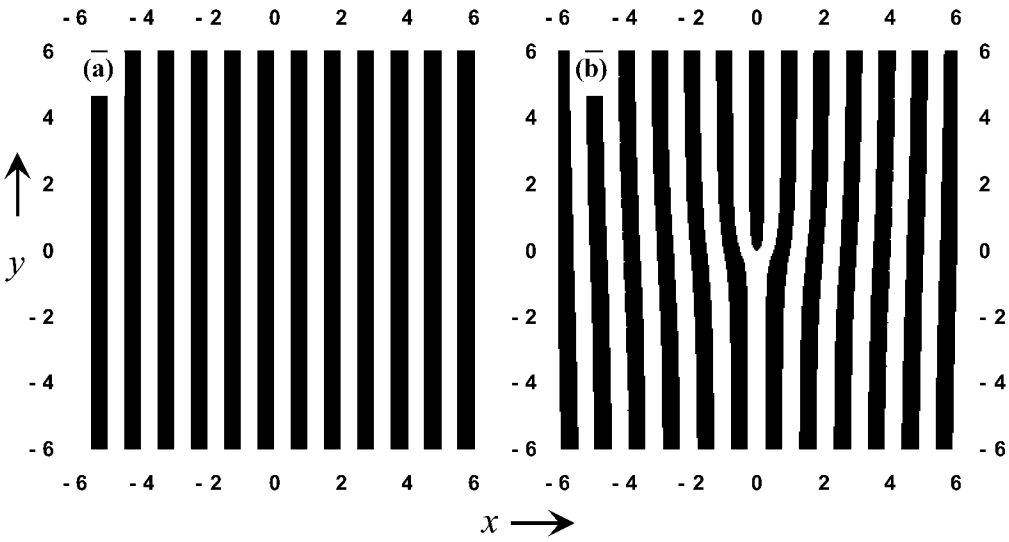

Fig. 2. Computer-generated binary patterns based on Eq. (1), for $K = 2\pi$. Each pattern consists of 1000×1000 pixels, with pixels for which $T = 0$ rendered black and $T = 1$, white. Pattern (a) has no encoded vortex ($M = 0$ in Eq. (1)). Pattern (b) has a single fringe bifurcation ($M = 1$); when used as a hologram it gives rise to vortices with topological charge ± 1 in the $\pm$first diffraction order.

2. Setup

The present technique is an adaptation of an already known holographic technique to create optical vortices in monochromatic laser light [8,9]. This technique uses binary transmission gratings defined by

$$T(x,y) = \begin{cases} 1 & \text{if } \sin(M\varphi - Kx) \geq 0 \\ 0 & \text{if } \sin(M\varphi - Kx) < 0 \,. \end{cases} \tag{1}$$

#7943 - $15.00 USD Received 1 July 2005; revised 9 September 2005; 12 September 2005
(C) 2005 OSA

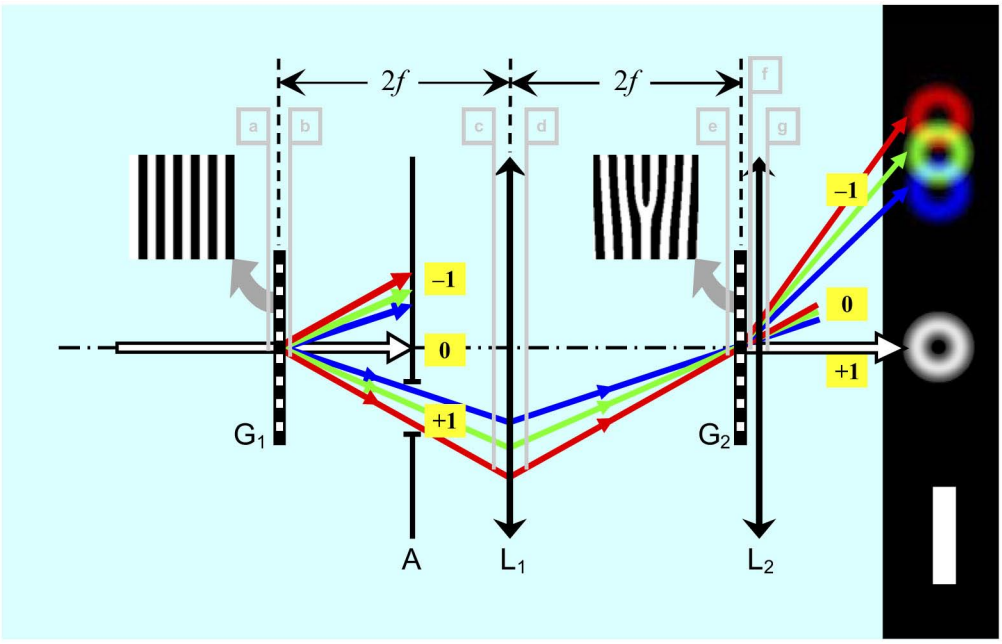

Fig. 3. Schematic of our $2f$ - $2f$ setup (not to scale). Ultrashort pulses enter from the left, and then pass through the following optical elements: G_1 = line grating without vortex fingerprint (see inset); A = order-selecting aperture; L_1 = planoconvex lens with focal length f; G_2 = grating with vortex fingerprint (see inset); L_2 = same as L_1. Diffraction orders (–1, 0, +1) are indicated as black numbers on a yellow background. The positions labeled with boxed lowercase letters (a … g) in light gray are used in our wavefront calculations (see Sec. 3). A few colored rays are shown to remind the reader that there is spatial chirp; white solid arrows indicate spatial chirp is absent. The artist's impressions on the right suggest the resulting far-field radiation: the +1 diffraction order from G_2 gives a spatial-chirp-free donut mode (white ring), while the –1 diffraction order suffers from spatial chirp. Note that we show just three colors—in reality, the frequency spectrum is of course continuous.

with x and y Cartesian coordinates in the grating plane, φ an azimuthal angle in the same plane ($\tan\varphi = y/x$), and M an integer. The grating constant Λ is determined by $K = 2\pi/\Lambda$. Figure 2(b) shows a 1000×1000 pixel sampled version of such a binary pattern for $M = 1$ and $K = 2\pi$ (so $\Lambda = 1$), with pixels with $T = 0$ rendered black, and pixels with $T = 1$, white. The key feature of this class of gratings is their fringe bifurcation (multifurcation) in the center: the top half of the pattern contains M more fringes than the bottom half. When such a grating is illuminated with a monochromatic wave having a Gaussian spatial profile, a superposition of Laguerre-Gaussian modes $LG_p^{\ell=\pm M}$ (ℓ is the azimuthal index) is produced in the $\pm$ first diffraction order [10]. The multifurcation in these gratings is thus the fingerprint of a vortex with topological charge M. Unfortunately, this single-grating method to generate optical vortices fails for broadband radiation (ultrashort pulses). In essence, each of the spectral components present in broadband radiation forms a good vortex in itself, but these vortices all travel in different lateral directions, because the diffraction angle is wavelength dependent. This phenomenon, known as angular dispersion (angular chirp), limits the focusability of the resulting radiation pulse, which is undesirable for intense-field applications.

To bypass this adverse effect, our method of generating femtosecond vortices makes use of a *pair of gratings*: one defined by Eq. (1) with $M = 1$, which we will now label G_2, plus an

exact copy of it *without the vortex fingerprint* (so with $M = 0$), which we label G_1. This simple straight-line grating is shown in Fig. 2(a). We arrange the two gratings in a setup as shown in Fig. 3, letting the incoming optical pulse first pass through G_1. Using an off-center aperture (marked A in Fig. 3) we only allow the +1 diffraction order to propagate. This order has angular chirp. A converging lens, L_1, then focuses the optical wave on G_2, which contains the vortex fingerprint. This lens with focal length f is positioned so that there is a distance of $2f$ both between G_1 and L_1 and between L_1 and G_2. A second lens, L_2, identical to L_1, is positioned immediately behind G_2. Having a linear magnification of -1, this telescope configuration allows us to preserve the beam collimation. Note that both L_1 and L_2 are centered on the optical axis, which also passes through the center of G_2 (the origin in Fig. 2(b)). As the colored rays drawn in Fig. 3 suggest, the angular chirp appearing behind G_1 can be undone by refocusing the radiation on G_2: each spectral component now approaches G_2 with precisely the angle required to make it coincide with the optical axis after diffraction by G_2. As a result, a broadband optical vortex without angular chirp emerges from the setup on the optical axis behind G_2. A strict mathematical proof of these statements based on the Kirchhoff-Fresnel diffraction integral formalism is presented in Sec. 3.

To improve the efficiency of our setup we could have used phase holograms instead of transmission holograms. However, we decided to ignore this and other efficiency-related issues like blazing in this paper, as its purpose is merely to demonstrate the technique that creates ultrashort pulses with vortices. For the same reason, we also leave aside the issue of Laguerre-Gaussian mode purity [11].

3. Wavefront propagation

In this section we wish to demonstrate theoretically that our setup (see Fig. 3) indeed produces a spatial-chirp-free optical vortex in an ultrashort pulse. We assume that an ultrashort pulse with a Gaussian spatial profile approaches the system in Fig. 3 from the left. We will follow the propagation of each monochromatic spectral component with wavenumber k separately, and find that the emerging wave is the same for all spectral components. To propagate the individual spectral components, we use the Kirchhoff-Fresnel integral formalism. Below, we use the subscripts a … f to denote the wavefront at various positions in the setup; these positions are marked with the corresponding boxed lowercase letters in Fig. 3. In the calculations we refer to the coordinate system shown in Fig. 2 and used in Eq. (1), and take the z axis to coincide with the optical axis.

To begin with, we have the incoming wave's electrical field with a Gaussian spatial profile of waist size w_0:

$$E_{\mathrm{a}} \propto \exp\left[-\frac{x^2}{w_0^{\,2}}\right]\exp\left[-\frac{y^2}{w_0^{\,2}}\right]. \tag{2}$$

Because G_1 is only modulated in the x direction and we have unit magnification, the wavefront immediately in front of G_2 will have exactly the same y dependence. Thus, we will suppress all y-dependent factors in what follows, and concentrate on the propagation of the x-dependent factor (note that we can factorize the diffraction integral). After passing G_1 the electric field in the first diffraction order acquires an extra phase factor; we find

$$E_{\mathrm{b}} \propto \exp\left[-\frac{x^2}{w_0^{\,2}} + iKx\right] \tag{3}$$

in which $2\pi / K$ is the grating constant. This wave propagates over the distance $2f$ from G_1 to the lens L_1, at which it arrives as

Received 1 July 2005; revised 9 September 2005; 12 September 2005

$$E_c \propto \exp\left[\frac{\left(x-\frac{K}{k}2f\right)^2}{w_c^2}+\frac{ik}{2R_c}\left(x^2+\frac{K}{k}L_R{}^2\frac{x}{f}-\frac{K^2}{k^2}L_R{}^2\right)\right], \tag{4}$$

where k is the wavenumber, $w_c{}^2 = w_0{}^2\left(1+(2f/L_R)^2\right)$ is the current waist size, $R_c = 2f + L_R{}^2/2f$ is the current radius of the curvature, and the Rayleigh length is defined as $L_R = \frac{1}{2}kw_0{}^2$ [2]. The center of the Gaussian envelope has been laterally displaced to $x = (K/k)2f$, and this is nothing else but angular chirp. The lens L_1 then adds a quadratic phase $\exp[-ikx^2/2f]$ to the wave. Propagating further, the wavefront reaches G_2, where its size is back to the initial value w_0 and its radius of curvature becomes f:

$$E_c \propto \exp\left[-\frac{x^2}{w_0{}^2}\right]\exp\left[\frac{ik}{2f}x^2\right]\exp\left[-iKx\right]. \tag{5}$$

The $\exp[-iKx]$ phase component still indicates angular dispersion, but it has *changed sign* compared to E_b, the wavefront just behind G_1. Now the wave passes through G_2, which has the same grating constant as G_1, but unlike G_1 also features a fringe bifurcation: its transmission $T_2(x,y)$ is given by Eq. (1), with $M = 1$. The lens L_2 compensates for the quadratic phase factor the beam acquired during propagation. Restoring the y-dependence that we have been suppressing in our notation thus far, we get

$$E_g \propto \exp\left[-\frac{x^2+y^2}{w_0{}^2}\right]\exp\left[-iKx\right]T_2(x,y). \tag{6}$$

This wave now propagates freely, causing the various diffraction orders to separate in the far field. For the Nth diffraction order, this free propagation involves a phase factor

$$\exp[iN(Kx+\varphi)]. \tag{7}$$

Equations (6) and (7) bring us to the central point of this paper: in the $N = +1$ diffraction order behind G_2, a vortex with topological charge +1 is expected, *without angular dispersion*. The phase factors $\exp(-iKx)$ in Eq. (6) and $\exp(+iKx)$ from Eq. (7) with $N = +1$ cancel, eliminating spatial chirp altogether. Note that in the $N = -1$ diffraction order the amount of spatial chirp is doubled instead of eliminated. In the next section, we present experimental images of the ±1 diffraction orders that exhibit exactly these features (Figs. 4(c)–(d) below).

4. Experiment

In our experiments, we used a Ti:sapphire oscillator (Spectra-Physics Tsunami) which produces pulses with a duration of ~25 fs (bandwidth ~40 nm, centered around ~800 nm) when mode-locked. The average power emitted is ~500 mW and the repetition rate is ~75 MHz; this corresponds to a pulse energy of ~7 nJ/pulse. To study the effects of bandwidth we also used the laser free-running (no mode-locking), in which case the bandwidth is reduced to

Received 1 July 2005; revised 9 September 2005; 12 September 2005

much less than 1 nm (close to a single 0.44-nm bin of our Ocean Optics spectrometer, which maps wavelengths in the range 200–1100 nm on a 2048-pixel CCD array).

The lenses L_1 and L_2 were identical plano-convex BK-7 lenses with nominal focal length $f = 300$ mm and diameter 50.8 mm. These lenses were anti-reflection coated for 800 nm.

For the gratings, paper printouts of computer-generated black-and-white patterns similar to those shown in Fig. 2 were photographed on black-and-white photo-film (Agfa APX-100). We used the developed negatives as our binary holograms G_1 and G_2. The holograms had a grating period $\Lambda = (51.4 \pm 0.7)$ μm (or approx. 20 lp/mm), making the first-order diffraction angle equal to 0.89° (for 800 nm). Using a knife-edge method, we determined that the diameter of our incoming beam was 2.0 mm (full width at the $1/e^2$ level, assuming a Gaussian profile), so that it illuminated approximately 40 linepairs of the grating. To avoid damage to the first holographic grating, G_1, we had to attenuate the incoming pulses by a factor of 100 using a neutral density filter.

Images were recorded by letting the resulting far-field radiation fall directly on the CCD chip of a camera, without using an objective. This camera was positioned 55 cm behind G_2 and was connected to a lab PC with a 10-bit camera interface plus software (Spiricon). We recorded single frames, with a shutter time of 1/60 s. We subtracted background images that were recorded with the laser beam blocked.

Figure 4 shows the images obtained. The top row panels, Figs. 4(a) and 4(b), were recorded with the laser free-running (narrowband spectrum), and the bottom row panels, Figs. 4(c) and 4(d), with the laser mode-locked (femtosecond pulses, broadband spectrum). In each of these rows, the left panels, Figs. 4(a) and 4(c), show the diffraction order we called $N = -1$ in the previous section; this is the order for which angular chirp is not expected to be compensated. The right panels, Figs. 4(b) and 4(d), show the diffraction order $N = +1$, for which angular chirp is expected to be eliminated. Each of the four panels is surrounded by graphs showing the intensity recorded along the horizontal and vertical lines indicated in the images.

As expected, the images in the free-running case show no noticeable difference between the orders $N = -1$, Fig. 4(a), and $N = +1$, Fig. 4(b). When the laser is free-running, the radiation is essentially monochromatic, so that the concept of spatial chirp becomes irrelevant. When the laser is mode-locked, however, the two diffraction orders are different. As expected, a blurred image is found for $N = -1$, Fig. 4(c): due to angular chirp, the clean dark center that was observable in the free-running case is no longer present. Figure 4(d) shows that the setup successfully eliminates spatial chirp in the mode-locked case in the order $N = +1$. In spite of the 40-nm bandwidth of our pulses, a clean dark spot results in the center of the image. (Because we subtract background images, pixels may record net negative values due to noise; in Fig. 4, these pixels are gray. We find such negative values far away from the center but also in the center.)

One question remains to be answered: does the donut mode shown in Fig. 4(d) really contain a vortex, i.e. an azimuthal phase structure given by $\exp(i\varphi)$? This can be investigated by overlapping this donut mode with some (planar or spherical) reference wavefront which contains no vortex, and recording the resulting interferogram. Bazhenov, Vasnetsov, and Soskin, early pioneers in optical vortex research, used this technique to demonstrate vortices in monochromatic light [8]. In our case, however, there is one complication: because we are dealing with ultrashort pulses, temporal overlap is an additional requirement for interference. Fortunately, our setup offers an elegant solution to this problem in the form of the zero-order radiation coming out of G_1. Upon arrival at G_2/L_2 this radiation is inherently synchronous with the first-order vortex-containing donut mode; this follows directly from an application of Fermat's principle to our image-forming telescope [12]. Conveniently, the zero-order radiation also lacks a vortex. We allowed both the zero-order and the first-order radiation to travel through the system by opening up the order-blocking aperture A in Fig. 3. Figure 5 shows the interferogram we then recorded. To get good fringe visibility, we found we needed

to reduce the intensity of the zero-order radiation substantially. We could not do this using an attenuation filter in the zero-order radiation because the resulting time delay between the zero-order and first-order radiation was large enough to spoil the interference pattern. Instead, we needed to attenuate the zero-order radiation while preserving its synchronicity with the vortex donut. To this end, we sent the zero-order radiation through a tiny pinhole pierced in a

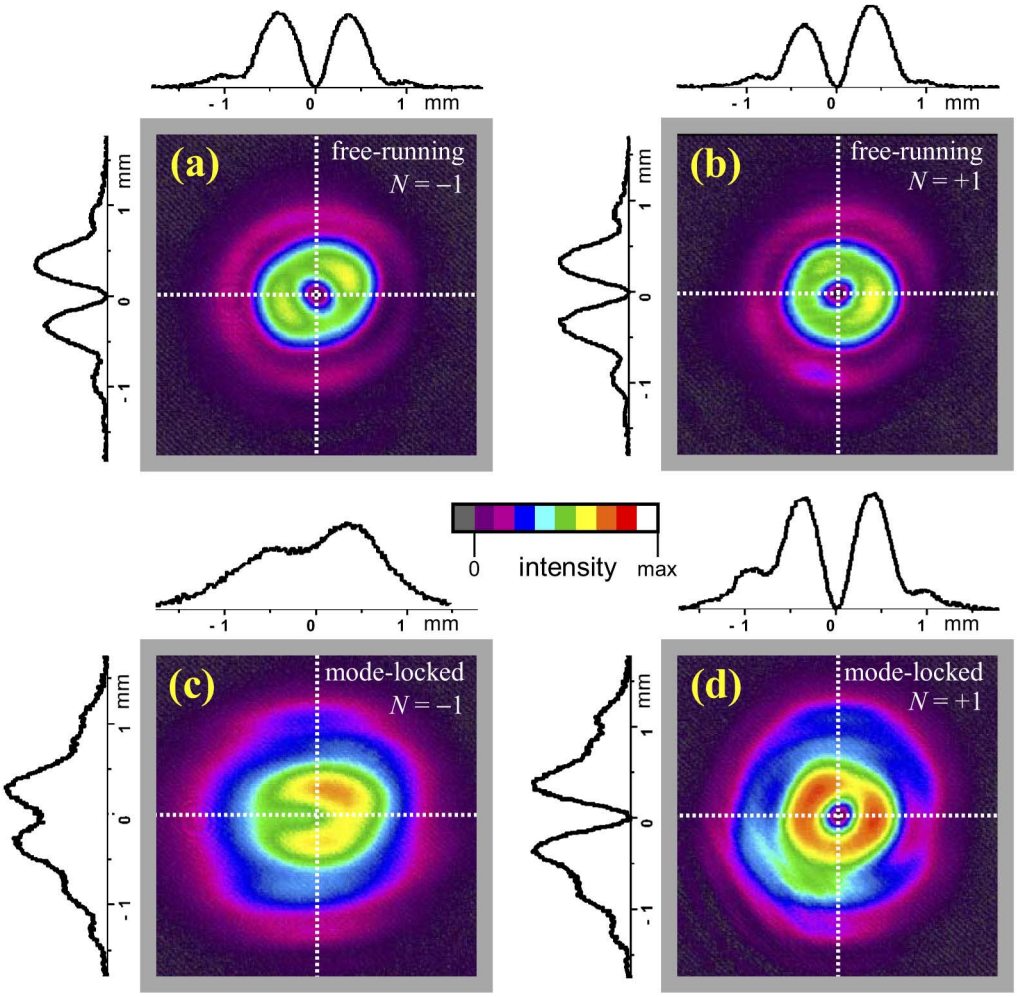

Fig. 4. Images of optical vortices. Intensities in arbitrary units as indicated by the color bar in the center (negative values resulting from background subtraction are indicated in gray). Top row: laser free-running (narrowband radiation). Bottom row: laser mode-locked (femtosecond pulses, broadband radiation). Left column: no compensation of spatial chirp (diffraction order $N = -1$). Right column: spatial chirp compensated (diffraction order $N = +1$). The line graphs above and to the left of each image show the intensity distributions (in arbitrary units) along the horizontal and vertical dotted lines. Note the clean dark center in panel (d), and its absence in panel (c) due to spatial chirp. See Sec. 4 for more details.

#7943 - $15.00 USD Received 1 July 2005; revised 9 September 2005; 12 September 2005
(C) 2005 OSA

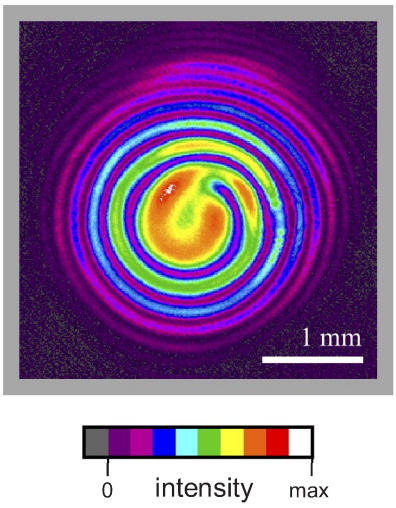

Fig. 5. Interferogram of an ultrashort optical vortex. To obtain this image, we let the chirp-free optical vortex-containing donut mode as shown in Fig. 4(d) interfere with a vortex-free spherical reference wave. This reference wave was created by allowing the zero-order radiation coming from grating G_1 (see Fig. 3) to propagate through the setup. To get good fringe visibility, we attenuated this reference wave by using a tiny pinhole (see text). A one-armed spiral can be recognized in the image, indicating that the topological charge of the vortex in our ultrashort pulse equals 1.

piece of opaque paper with a sharp needle. Of course, the diffraction of the zero-order radiation by this tiny pinhole will give it a radius of curvature that differs noticeably from that of the vortex donut. As is well-known from the CW vortex research, this gives rise to a spiral-like structure in the interferogram, exactly as we observe in Fig. 5 (which the reader may compare to Fig. 1(b) in Ref. [9]). In our case the observed spiral has a single arm, which indicates that our vortex has topological charge $m = 1$ [10]. All this confirms that the phase structure in our donut mode is indeed $\exp(i\varphi)$.

Finally, we estimated the pulse duration of our chirp-free vortex mode. To this end, we used a microscopy cover glass, Corning No. 1, with a thickness D falling between 130 μm and 160 μm [13]. We observed that the interference pattern disappears completely when we hold this cover glass in the zero-order radiation, but that it *reappears* when both the zero-order and the first-order are sent through it. The time delay Δt that the cover glass introduces between the zero-order and first-order radiation when only the zero-order radiation is sent through it equals

$$\Delta t = \frac{D}{c/n} - \frac{D}{c} = \frac{D}{c}(n-1) \tag{8}$$

in which c is the speed of light in vacuum (or air), and n the group index of refraction (speed of light in vacuum divided by the group velocity) of the cover glass material. Because this delay causes the interference pattern to disappear, it must be an upper limit for the pulse duration of our produced chirp-free vortex mode. We get a value of 280 fs for this upper limit when we set $D = 160\,\mu\text{m}$ and $n = 1.523$ in Eq. (8). This value of 280 fs is conservative because the cover glass we used may be thinner, and because the value 1.523 for n is the phase index of refraction of the cover glass material at the sodium D line, 589 nm [13]. For 800 nm we expect a lower phase index, and, furthermore, the group index of glasses is usually

lower than their phase index. We also recorded the spectrum of our vortex mode, and noted that it is similar in width to the Ti:sapphire oscillator's spectrum. Probably the duration of our vortex mode is limited by the GVD of the BK-7 lenses to a value of ~ 60 fs, but this limit could easily be circumvented with thinner lenses.

To the best of our knowledge, our interferogram in Fig. 5 is the first one ever published of a vortex of femtosecond duration.

5. Conclusions

We have demonstrated that our $2f$ - $2f$ setup can produce an optical vortex in ultrashort radiation pulses. In fact, our wavefront calculations suggest that we should be able to generate virtually any light structure, as long as we can encode it in a computer-generated hologram.

Apart from the two home-made computer-generated holograms, our setup consists of readily available (and inexpensive) optical components. It is easily aligned: we used a ruler to position the optical elements properly and a CCD camera to align the beam onto the holograms. Alignment seems to be a crucial issue for the perfection of a $4f$ scheme [7]. The telescope in that scheme requires precise alignment, while in our $2f$ - $2f$ setup the telescope alignment only influences the beam divergence, leaving the angular dispersion unaffected. The purpose of our lens L_2 is to restore the collimation of the beam; it can be replaced with another lens if needed.

Our setup currently produces only weak vortex-carrying pulses. Its efficiency can certainly be improved by using phase holograms instead of transmission holograms, and also by blazing. Ultimately, a more flexible option is to use a PC-controlled spatial light modulator in conjunction with an adaptive learning algorithm [14]. This will allow us to simultaneously optimize the energy efficiency of our setup and, if desired, the mode purity of the produced vortex pulse.

Acknowledgments

The authors would like to thank H. Batelaan, A. Khizhnyak, and M. Vasnetsov for stimulating discussions. This work was supported in part by the National Science Foundation (Award No. PHY-0355235). I.G.M. (on leave from Institute of Physics, NAS of Ukraine) gratefully acknowledges support by a Theodore P. Jorgensen Postdoctoral Fellowship from the AMO Physics Priority Initiative of UNL.

Note added in proof - Using two equally thick cover slips and tilting one, we have now determined a 66-fs upper limit for the duration of the vortex-containing pulse (cf. Sec. 4).

Received 1 July 2005; revised 9 September 2005; 12 September 2005